Sensor Applications

60 GHz FMCW Millimeter Wave Radar Assisted with Dual-Layer Wideband Flexible Metasurface for Accurate Wrist Pulse Monitoring

Rifa Atul Izza Asyari[1*], M. Zharfan Wiranata [2], Roy B. V. B. Simorangkir [3], Daniel Teichmann [4], Changzhi Li [5]
1,2 Student Member, IEEE, 3,5 Member, IEEE, 5 Fellow, IEEE

Abstract—This paper presents a novel passive focusing metasurface designed for wrist pulse detection within the 60 GHz millimeter wave frequency range, incorporating a dual-layer transmitarray antenna. The proposed metasurface demonstrates exceptional polarization characteristics and a high degree of operational efficiency, as substantiated by rigorous far-field assessments. This innovative metasurface has significant potential for applications in human-device interfaces, health monitoring systems, and safety screening protocols, where the ability to focus and manipulate waves with flexibility is paramount. We rigorously evaluated its radiative safety and compared its efficacy with a conventional photoplethysmogram (PPG) reference. The results show a close agreement between our proposed design and the PPG.

Index Terms—FMCW, Radar, Wrist Pulse, PPG

I. INTRODUCTION

Wearable devices designed for continuous physiological monitoring, particularly heart rate and blood pressure, have garnered significant scientific interest [1]. Their ability to quickly detect conditions such as cardiac arrhythmias and hypertension, which are indicative of broader cardiovascular issues, represents a significant advancement in public health. Various technologies, such as electrocardiogram (ECG) [2], photoplethysmogram (PPG) [3], ballistocardiogram (BCG) [4], and tonometry [5], have been investigated for noninvasive, continuous blood pressure measurement in daily life and medical settings. Much of the research centers on capturing arterial pulsations and generating precise pulse signals.

Innovative studies have ventured into the application of microwave frequencies to the study of arterial pulses. For instance, Jessi et al. [6] introduced an antenna concept within the millimeter-wave Frequency-Modulated Continuous Wave (FMCW) radar framework for arterial pulse waveform detection, with the potential to yield high-quality measurements suitable for characterizing Pulse Wave Analysis (PWA) and Pulse Transit Time (PTT) for blood pressure monitoring. Kim et al. [7] suggested a wrist pulse detector using an injection-locked Phase-Locked Loop (PLL) mechanism. Their novel approach harnesses the idea of near-field coupling between a flat resonator and the radial artery of the wrist. In a different approach, Tang et al. [8] presented a wrist-mounted sensor that combines a range-correlated continuous wave radar (RC-CW) with a self-injection-locked radar (SIL-CW) to simultaneously monitor chest cardiac pulsations and radial wrist pulse movements. Additionally, various methods utilizing proximity coupling RF sensors [9], microwave near-field self-injection locking techniques [10], and wrist pulse detection sensors based on array resonators [11] [12] [13] have been explored, and preliminary studies have shown promise in radar-based pulse pressure analysis [14]. However, a significant limitation observed is the need for a stabilizing handgrip, which can be problematic in real-world applications. Furthermore, the accuracy and reliability of this method still require validation.

Radar-based techniques non-invasively and discreetly monitor vital signs, yet they typically require setups close to the body, where skin-mounted sensors can interfere with natural movement, impacting measurement accuracy. Additionally, these methods rely heavily on battery life. Acknowledging these challenges, our research advocates for the promising of a non-contact millimeter-wave radar passive technique to capture arterial pulse waveforms.

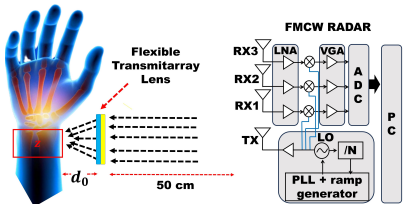

Fig. 1. Illustration of the proposed metasurface-assisted mm-Wave radar system.

This approach has the potential to provide highly accurate readings essential for Pulse-Wave Analysis (PWA) and Pulse Transit Time (PTT), particularly in the context of blood pressure monitoring. Our research introduces an innovative approach by incorporating a transmitarray lens into a wrist pulse detection system operating in the millimeter-wave GHz, as illustrated in Fig. 1. This implementation is designed to enhance the sensitivity of the system by stabilizing and concentrating the emitted radar wave. Our comprehensive evaluation includes a comprehensive performance evaluation against established benchmarks in photoplethysmography (PPG), highlighting potential advancements in wrist pulse detection enabled by our transmitarray lens technology.

II. TRANSMITARRAY DESIGN

In this research, we exploit the distinct properties of the transmitarray lens, which allows meticulous control over the phase, amplitude, and polarization of electromagnetic wavefronts. This capability is crucial for accurately focusing the radar beam on the target area, specifically the wrist. The design of the transmitarray lens unit cell, illustrated in Fig. 2, features a square configuration with each side measuring W = 1.6 mm which corresponds to approximately $0.6\lambda_g$ within the material, considering the dielectric properties of the

Corresponding author: Rifa Atul Izza Asyari (e-mail: raia@mmmi.sdu.dk)

substrate. Here, λ_g denotes the wavelength in the medium, which is influenced by the dielectric constant of the substrate (ε_r).

A polyimide film has been chosen as a substrate, characterized by a dielectric constant of ε_r = 3.5. At 60 GHz, the free space wavelength λ_o is around 5 mm, leading to an adjusted wavelength in the medium (λ_g) of about 2.67 mm, derived from $\lambda_g = \lambda_o/\sqrt{\varepsilon_r}$. Therefore, the chosen unit cell dimension of 1.6 mm aligns with $0.6\lambda_g$ on the polyimide substrate, a vital factor for the performance, efficiency and manipulation of the electromagnetic wave.

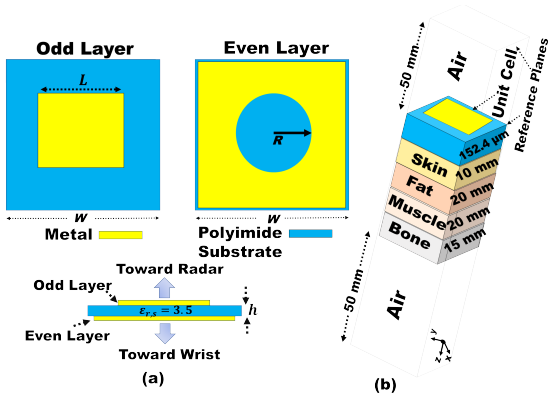

Fig. 2. (a) Unit cell design of the transmitarray lens. (b) unit cell setup in HFSS taking into account the human phantom model.

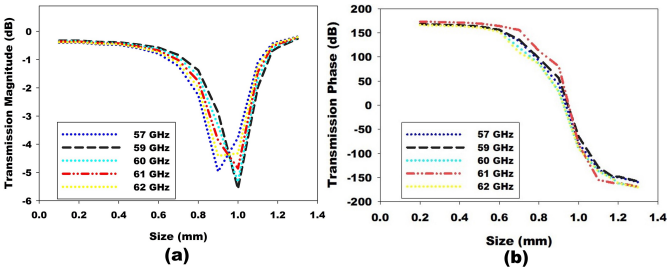

Fig. 3. Transmission response at frequency 57 - 62 GHz: (a) Transmission magnitude from unit cell (L = 0.15-1.4 mm, W = 1.6 mm, R = 0.6 mm. (b) transmission phase.

The design and optimization of the transmitarray lens were performed with ANSYS HFSS software, employing periodic boundary conditions and Floquet port excitations. The even layer features a square copper with ($\sigma = 5.8E+007S/m$) which is about 35μm thick etched on polyimide films with a circular hole , whereas the odd layer exhibits a square pattern copper positioned on the opposite side of the circular hole. The simulations incorporated a human tissue model with a 10 mm thick skin layer ε_r = 35, 20 mm of fat ε_r = 9, 20 mm of muscle ε_r = 52, and 15 mm of bone ε_r = 14 [15].

In Figures 3 (a) and 3 (b), we observe the transmission magnitudes and phases at 60 GHz as functions of the units of cells, L and R. Our objective was twofold: first, to identify the optimal dimensions for achieving a target transmission magnitude of −3 dB and a transmission phase of 350°, with the 0° phases serving as the focusing beam; and second, to determine the range of viable parameters during our optimization process. The adjustment of L, which varies between 0.2 and 1.2 mm, yields the relevant transmission characteristics of the element at 60GHz. However, the 350° phase change is consistently illustrated at various frequencies, underscoring the wideband adaptability of our proposed structure, and presents the transmission magnitudes at various frequency points for a specific unit cell dimensions.

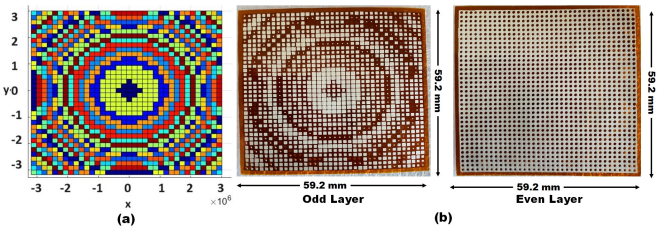

Fig. 4. (a) Optimization structure of flexible transmission metasurface using Matlab (b) Printed flexible transmitarray lens Odd-layer and Even-layer.

Building on these findings, we then explore the concept of non-uniform transmitarray lens configurations. The rationale behind this approach is rooted in our aim of achieving a uniform phase 0° distribution across a finite-size transmitarray lens, which is critical for optimal directivity and beam focus. One of the core challenges here is to ensure phase corrections through strategic modifications of unit cells. Figure 4 (a) displays a meticulously crafted beam-focusing transmitarray lens optimized with MATLAB for precise electromagnetic interactions. This state-of-the-art design, fabricated on a flexible polyimide substrate as shown in Figure 4 (b), comprises 37x37 elements spread over an area of 59.2 mm x 59.2 mm, specifically designed for operation at 60 GHz. Such a transmitarray lens, operating in the millimeter-wave spectrum, offers significant potential for medical and radar applications, where the ability to focus and manipulate waves with flexibility is paramount.

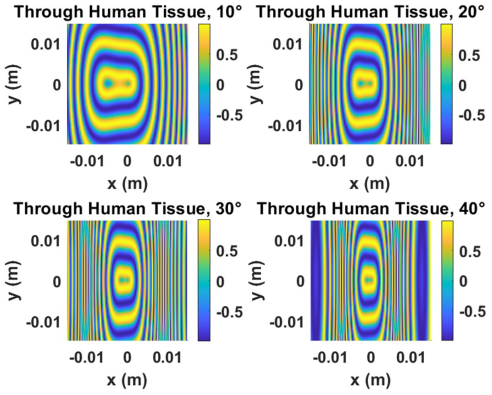

Fig. 5. Different bending condition 10°, 20°, 30°, and 40° through human tissue of flexible transmitarray lens.

In Figure 5 graphically demonstrate the focusing capabilities of a transmitarray lens when directing electromagnetic waves through human tissue to different bending angles ranging from 10° to 40°. The coordinates of any element on the focused transmitarray can be expressed as (x_{ij}, y_{ij}) and the focal length is recorded as F_t, the transmission phase difference $\Delta\varphi_i$ for the i th element is shown in equation (1).

$$\Delta\varphi_i = 2 \cdot k \cdot \left(\sqrt{R_i^2 + F_t^2} - F_t\right) \tag{1}$$

$$R_i = \sqrt{x_{ij}^2 + y_{ij}^2} \tag{2}$$

where k is the propagation constant and Equation (2) denotes the distance from the center of the focused transmit array to any element. The color gradients indicative of the intensity of the electric field within the tissue, measured in volts per meter (V/m). Intensity modulation, from cooler to warmer hues, encapsulates the field amplification under the influence of the lens [16]. Notably, the convergence of the wave, as dictated by the transmitarray lens, deviates significantly from its natural linear progression in free space, underscoring the efficacy of the lens in achieving a localized focus within the tissue.

III. WRIST PULSE RADAR DETECTION

In our study, we employed the BGT60TR13C FMCW radar sensor provided by Infineon Technologies. This RF front-end chipset operates in a frequency range of 58 to 63.5 GHz and is equipped with one transmitter and three receivers. The experimental setup, comprising both the radar and our modifiable transmitarray lens affixed to the wrist, is illustrated in Figure 6.

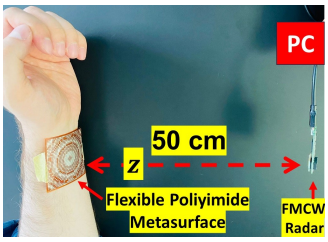

Fig. 6. Experimental setup for FMCW Radar with Flexible transmitarray lens

The experiments were carried out to collect physiological signals, as depicted in Figure 6. Throughout these studies, four participants were instructed to relax and breathe naturally while wearing a flexible transmitarray lens on their wrists, all in proximity to the FMCW radar and while equipped with a flexible lens. Due to variations in the structure of the human body and the lightweight, thin, and flexible nature of our transmitarray lens, it could bend between 5^o and 15^o without compromising the antenna performance or the precision of vital sign detection. The signal transmitted by the FMCW radar can be defined in the following manner:

$$S_{Tx}(t) = \exp\left[j\left(2\pi f_c t + \pi \frac{B}{T_f} t^2 + \varphi(t)\right)\right] \tag{3}$$

where f_c denote the center frequency, B represents the signal's bandwidth, T_f stands for the ramp duration, T_i signify the frame duration of the emitted signal, and $\varphi(t)$ indicate the starting phase of the signal. Given that wrist movement can be likened to a basic harmonic motion, the gap between the antenna and the human wrist surface can be described as

$$R(\tau) = d_0 + A\sin(2\pi f_r \tau) + B\sin(2\pi f_h \tau) \tag{4}$$

where d_0 is the gap between the antenna and the wrist, A and B depict the peak amplitude of the wrist pulse, f_r and f_h stand for the breathing and heart rates, respectively. The duration of a chirp is very short, and d_0 is considered constant during a chirp. The signal captured at this moment when it is reflected from the human wrist can be described in the following manner:

$$\begin{aligned} S_{Rx}(t) &= \exp\left[j\left(2\pi f_c\,(t-t_d) + \pi\frac{B}{T_f}\,(t-t_d)^2 + \varphi\,(t-t_d)\right)\right] \\ t_d &= \frac{2R(\tau)}{c} \end{aligned} \tag{5}$$

$$\begin{aligned} x(t) = S_{Tx}(t) * S_{Rx}(t) &\approx \exp\left[j\left(4\pi\frac{BR(\tau)}{cT_f}t + \frac{4\pi f_c R(\tau)}{c}\right)\right] \\ &= \exp\left[j\,(f_b t + \varphi_b)\right] \\ f_b &= \frac{2BR(\tau)}{cT_f} \\ \varphi_b &= \frac{4\pi f_c R(\tau)}{c} = \frac{4\pi R(\tau)}{\lambda} \end{aligned} \tag{6}$$

Where c is the speed of light, φ_b indicates the phase of the IF signal, f_b is the frequency of the IF signal $x(t)$. The displacement data $R(\tau)$ of the human wrist are embedded in both f_b and φ_b. Given that wrist movement due to pulse wave is minimal, falling below the radar range resolution, it is not feasible to determine wrist displacement from f_b. Therefore, the displacement of the wrist must be derived from φ_b, with greater precision achieved for shorter wave lengths.

IV. RESULTS

To extract the pulse signal derived from the FMCW radar, we advocate the Ensemble Empirical Mode Decomposition (EEMD) for processing and to opt for IMF components spectral peaks within the 0.9-2Hz bandwidth, specifically tailored for the reiteration of the quintessential heartbeat signal.

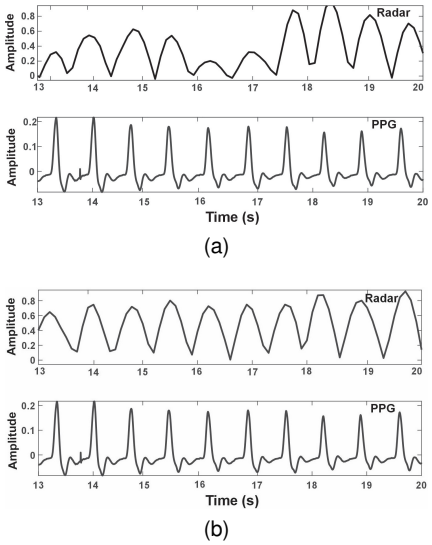

Fig. 7. Comparison of the extracted radar wrist pulse and PPG signal (a) without flexible transmitarray lens (b) with flexible transmitarray lens.

A comprehensive spectral analysis of these refined heartbeat signals facilitates the determination of precise heartbeat rates. Figure 7 provides a visual comparison of the wristpulse waveforms obtained from the radar, both with and without our adaptable lens. Figure 7 (a) presents the standardized pulse waveform obtained without our adaptable lens. On the other hand, Figure 7 (b) depicts the

standardized heartbeat waveform captured with our adaptable lens in operation. The data show notable enhancement and stabilization of the heartbeat waveform when the flexible transmit array is used compared to that without the use of an adaptable lens.

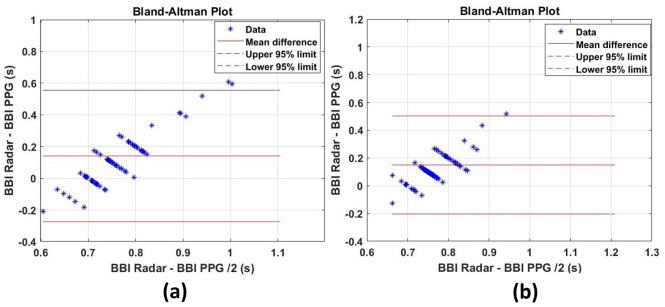

Fig. 8. Bland Altman plot comparison of the extracted Beat-Beat Interval (BBI) radar and PPG (a) without flexible transmitarray (b) with Flexible transmitarray

Figure 8 presents the Bland-Altman plots, which compare the beat-to-beat intervals measured by the Radar and PPG techniques. The mean differences between these two methods are represented by solid red lines. In addition to the mean, the black dashed lines enclose the upper and lower limits of agreement 95%. These boundaries are calculated by adjusting the mean difference by ±1.96 times the standard deviation of the discrepancies, thus defining the expected range for most comparative measurement variances. A detailed review of the plots reveals a consistent offset; specifically, Figure 8 (a) shows a slight systematic underestimation of -3.623 ms by the Radar method, while figure 8 (b) indicates a slight overestimation of 2.252 ms. These biases, contained within the dashed lines, provide information on the alignment of the two measurement techniques.

TABLE 1. Mean Accuracy Results for Five Subjects with and without a Flexible Transmitarray Lens on a Wrist Pulse

Subject	With Flexible Metasurface					Without Flexible Metasurface				
	AVG (ms)		SDNN (ms)		ACC (%)	AVG (ms)		SDNN (ms)		ACC (%)
	Radar	PPG	Radar	PPG		Radar	PPG	Radar	PPG	
1	704.1	705.4	37.2	37.3	97.13	694.1	706.12	41.13	39.3	96.59
2	695.2	693.4	42.3	41.8	97.33	705.2	713.45	43.3	44.27	96.11
3	755.8	760.7	56.9	57.5	96.62	705.8	720.9	49.8	52.5	96.62
4	705.9	710.1	38.1	39.1	96.35	675.9	711.1	45.1	45.7	95.77
5	781.8	783.3	49.5	49.8	97.19	731.37	767.1	56.6	57.3	97.20

Table 1 presents detailed results of short-term wrist pulse measurements taken for a duration of 60 seconds for five subjects, using both a flexible metasurface and a standard PPG. The table compares the average beat-to-beat intervals (AVG), the standard deviation of the NN intervals (SDNN), and the accuracy percentages (ACC) for both methods. It illustrates that the use of flexible transmitarray in measurements aligns closely with the PPG results and has better accuracy , showing no significant discrepancy in SDNN values and a relative error of less than 7.09% for SDNN, indicating its effectiveness for a quick and sensitive BBI analysis.

V. CONCLUSION

We have introduced a groundbreaking introduces a dual-layer wideband flexible transmitarray that is efficient and increases sensitivity. The essence of our design lies in a compact element that boasts two copper layers printed on a single-layer substrate. This innovative structure achieves an extensive 350° phase coverage, facilitated by the physical rotation of the element, with a remarkable transmission efficiency where signal loss is maintained at better than -3 dB. This balance between wide phase coverage and minimal signal loss underscores the efficacy of our design strategy. The results show a close agreement between the flexible wrist pulse radar transmitarray lens with the PPG comparison. This configuration has the potential to be integrated into modern communication devices and the suggested sensor emerges as a promising option for non-invasive wrist pulse detection, potentially paving the way for new applications in health monitoring technologies.

REFERENCES

[1] Park, S. and Jayaraman, S., 2003. Enhancing the quality of life through wearable technology. IEEE Engineering in medicine and biology magazine, 22(3), pp.41-48.

[2] Israel, S.A., Irvine, J.M., Cheng, A., Wiederhold, M.D. and Wiederhold, B.K., 2005. ECG to identify individuals. Pattern recognition, 38(1), pp.133-142.

[3] Temko, A., 2017. Accurate heart rate monitoring during physical exercises using PPG. IEEE Transactions on Biomedical Engineering, 64(9), pp.2016-2024.

[4] P. Yousefian et al., "Pulse Transit Time-Pulse Wave Analysis Fusion Based on Wearable Wrist Ballistocardiogram for Cuff-Less Blood Pressure Trend Tracking," in IEEE Access, vol. 8, pp. 138077-138087, 2020, doi: 10.1109/ACCESS.2020.3012384.

[5] Sato, T., Nishinaga, M., Kawamoto, A., Ozawa, T. and Takatsuji, H., 1993. Accuracy of a continuous blood pressure monitor based on arterial tonometry. Hypertension, 21(6pt1), pp.866-874.

[6] J. E. Johnson, O. Shay, C. Kim and C. Liao, "Wearable Millimeter-Wave Device for Contactless Measurement of Arterial Pulses," in IEEE Transactions on Biomedical Circuits and Systems, vol. 13, no. 6, pp. 1525-1534, Dec. 2019, doi: 10.1109/TBCAS.2019.2948581.

[7] J. M. Kang, T. Yoo and H. C. Kim, "A Wrist-Worn Integrated Health Monitoring Instrument with a Tele-Reporting Device for Telemedicine and Telecare," in IEEE Transactions on Instrumentation and Measurement, vol. 55, no. 5, pp. 1655-1661, Oct. 2006, doi: 10.1109/TIM.2006.881035.

[8] B. -H. Kim et al., "A Proximity Coupling RF Sensor for Wrist Pulse Detection Based on Injection-Locked PLL," in IEEE Transactions on Microwave Theory and Techniques, vol. 64, no. 5, pp. 1667-1676, May 2016, doi: 10.1109/TMTT.2016.2549531.

[9] M. -C. Tang, C. -M. Liao, F. -K. Wang and T. -S. Horng, "Noncontact Pulse Transit Time Measurement Using a Single-Frequency Continuous-Wave Radar," 2018 IEEE/MTT-S International Microwave Symposium - IMS, Philadelphia, PA, USA, 2018, pp. 1409-1412, doi: 10.1109/MWSYM.2018.8439326.

[10] C. -H. Tseng, T. -J. Tseng and C. -Z. Wu, "Cuffless Blood Pressure Measurement Using a Microwave Near-Field Self-Injection-Locked Wrist Pulse Sensor," in IEEE Transactions on Microwave Theory and Techniques, vol. 68, no. 11, pp. 4865-4874, Nov. 2020, doi: 10.1109/TMTT.2020.3011446.

[11] Y. -J. An, B. -H. Kim, G. -H. Yun, S. -W. Kim, S. -B. Hong and J. -G. Yook, "Flexible Non-Constrained RF Wrist Pulse Detection Sensor Based on Array Resonators," in IEEE Transactions on Biomedical Circuits and Systems, vol. 10, no. 2, pp. 300-308, April 2016, doi: 10.1109/TBCAS.2015.2406776.

[12] C. -S. Lee, C. -Y. Wu and Y. -L. Kuo, "Wearable Bracelet Belt Resonators for Noncontact Wrist Location and Pulse Detection," in IEEE Transactions on Microwave Theory and Techniques, vol. 65, no. 11, pp. 4475-4482, Nov. 2017, doi: 10.1109/TMTT.2017.2684118.

[13] T. -J. Tseng and C. -H. Tseng, "Noncontact Wrist Pulse Waveform Detection Using 24-GHz Continuous-Wave Radar Sensor for Blood Pressure Estimation," 2020 IEEE/MTT-S International Microwave Symposium (IMS), Los Angeles, CA, USA, 2020, pp. 647-650, doi: 10.1109/IMS30576.2020.9224111.

[14] Y. Rong, K. V. Mishra and D. W. Bliss, "Radar-Based Radial Arterial Pulse Rate and Pulse Pressure Analysis," 2021 29th European Signal Processing Conference (EUSIPCO), Dublin, Ireland, 2021, pp. 1870-1874, doi: 10.23919/EUSIPCO54536.2021.9616318.

[15] Gabriel S, Lau RW, Gabriel C. The dielectric properties of biological tissues: III. Parametric models for the dielectric spectrum of tissues. Phys Med Biol. 1996 Nov;41(11):2271-93. doi: 10.1088/0031-9155/41/11/003. PMID: 8938026.

[16] S. Paul, N. K. Tiwari and M. J. Akhtar, "Design of Highly Directive GRIN MS Lens Integrated DFHA for Deep Tissue Biomedical Imaging," in IEEE Transactions on Antennas and Propagation, vol. 71, no. 1, pp. 330-341, Jan. 2023, doi: 10.1109/TAP.2022.3222808.